CONF-760209--2

IMPURITY AND SURFACE STUDIES IN ORMAK*

R. J. Colchin, C. E. Bush, G. L. Jahns, J. F. Lyon,
M. Murakami, R. V. Neidigh, and D. L. Shaeffer

Oak Ridge National Laboratory
Oak Ridge, Tennessee 37830, USA

Abstract

The ORMAK tokamak has been in operation since 1971, and surface impurity problems have been pursued from the beginning. Surface studies of materials removed from ORMAK have revealed the presence of C, O, and Fe. These are also the principal impurities observed spectroscopically in plasma discharges, although numerous other elements are present in lesser amounts. Spectroscopy, x-ray measurements, plasma resistance, and fast ion scattering have been used in an effort to determine Z_{eff}, the effective nuclear charge of plasma ions. All four measurements have practical difficulties leading to relatively large experimental error limits. Oxygen discharge pre-cleaning has allowed ORMAK discharges to reach higher currents and correspondingly higher ion and electron temperatures; spectroscopic studies reveal a lower level of contaminants, particularly C and N. Power measurements indicate that most of the input power strikes the walls, mostly as radiation. By varying operating parameters it is found that $Z_{eff} \sim I_p/\bar{n}_e$.

*Research sponsored by the Energy Research and Development Administration under contract with the Union Carbide Corporation.

1. Introduction

Surface and impurity problems have been actively pursued using the ORMAK tokamak since its inception. As a precaution against the adsorption of gases, the stainless steel walls of the liner were vacuum coated with a layer of platinum and gold [1,2], with the Pt acting as a seal to prevent impurities in the stainless steel from reaching the outer Au coating. In spite of such clean beginnings, the liner walls are presently contaminated with elements other than gold. Our understanding of this contamination is detailed in the next section. Details of the resulting plasma impurities and impurity measurements are given in Section 3. The consequences of oxygen discharge pre-cleaning are shown in Section 4, and Section 5 discusses measurements of power to the walls and impurity scaling.

2. Surface Contamination

Surface contamination on the walls of the ORMAK liner has been identified by visual inspection, by Auger electron spectroscopy (AES) of removed wall samples, and by in situ measurements using a soft x-ray appearance potential spectrometer (SXAPS). The SXAPS experiment is described in another paper [3].

Visible contamination arising from two sources has been identified. Near the limiter, gold on the walls is covered with tungsten, encompassing approximately a third of the surface area of the torus. Gold remains visible in areas shielded by small liner protrusions, indicating that tungsten has been deposited at grazing incidence to the walls. In the region of the Thomson scattering system, 180° away from the limiter, several dark areas are evident. Again, these dark areas are in slight depressions, between seams in the liner. They are centered about the

region of the laser viewing dump, which consists of tightly packed austenitic stainless steel razor blades. Liner samples taken from nearby show $\leq 50\%$ coverage with Fe, so that it is likely that the dark areas are deposits of iron.

Various plugs, lenses, and other parts of the first liner and the present (second) liner have been analyzed by AES. All such analyses involved exposure to air after removal from ORMAK, with probable accompanying surface contamination. Ion sputtering has been used to remove surface layers and thereby provide depth profiles. The principal contaminants found were C, O, and Fe [4].

3. ORMAK Plasma Contamination and Z_{eff}

The first indications of plasma impurities came from optical observations. The extent to which impurities cause energy loss and control plasma current profiles was rather dimly appreciated until three to four years ago. Since that time a lot of effort has been expended to identify and determine the amount of impurities in the plasma [5], the effect of impurities on both particle transport and energy loss, and the manner in which walls react with the plasma. Unfortunately, there is as yet no easy way to measure any of these phenomena, so that only partial answers are possible.

In fact, the determination of Z_{eff},

$$Z_{eff} = \sum_i n_i Z_i^2 / n_e ,$$

(i indicates ion species, n_i and n_e are ion and electron densities, Z_i is the charge state of the ion), by any of several means is not a simple task; and it is often difficult to determine whether a change in wall contamination (such as by oxygen discharge cleaning, discussed in Sect. 4)

increases or decreases Z_{eff}. Problems associated with the ways of measuring Z_{eff} are discussed below, along with experimental results.

Probably the most widely used method of plasma impurity identification (and hence Z_{eff} determination) is spectroscopy. Many impurity lines fall in the ultraviolet, so that vacuum ultraviolet as well as visible spectra must be observed. Most ionization states of plasma impurity atoms do not normally exist in nature (except perhaps in stars). Therefore, the radiation frequencies of all but the two lowest lying ionization levels are not known for most atoms. A few atoms, such as C, O, and Fe, have known ionization levels; and it is on such atoms that plasma impurity studies are based.

Besides the problem of knowing the expected radiation frequencies, there are several difficulties in spectroscopically determining the amount of various plasma impurity species. One such difficulty is establishing the excitation rates for optical transitions. Since these rates are not generally measured, they must be inferred by theoretical calculations. A second problem is the detection of lines which are of weak intensity because of a large number of transition possibilities. A third problem is spectrometer intensity calibration in the ultraviolet. A fourth is that of obtaining and unfolding spectral intensities as a function of radius. Taken together, these problems result in an uncertainty factor of ≤ 5 in determining the amount of impurities.

In spite of these difficulties, spectroscopy provides a unique tool for the identification of impurities. Impurity species present in ORMAK [6] are given in Table I, along with their likely origin and estimates of their abundance.

TABLE I.

Another diagnostic often used to determine Z_{eff} is some form of x-ray detector. X-ray emission comes from bremsstrahlung, recombination, and line radiation, i.e. free-free, free-bound, and bound-bound electron transitions. The intensity of the bremsstrahlung radiation is proportional to $\sum_i n_i n_e Z_i^2$ [7], so the bulk of the radiation is emitted from the region of highest density. In practice most x-rays come from a small volume, making this a "point" measurement.

If bremsstrahlung were the only photon-producing process, measurement of the absolute intensity of x-rays emitted from a given volume would give Z_{eff} directly, provided n_e and T_e were known. Unfortunately, recombination radiation is usually more intense than bremsstrahlung; this indicates a need to know which impurities are present and what their charge states are as a function of radius. Thus the answer one gets depends on the assumed impurities. Another problem arises when runaway electrons are present. Photons generated by the runaways can add a high energy tail to the x-ray spectrum which has nothing to do with impurities. Line radiation from bound-bound transitions represents still another complication, and signals from such transitions must be subtracted if present.

X-ray measurements of Z_{eff} have been made in ORMAK using both a soft x-ray detector [8] and a PIN diode array. The latter detector gives spatially resolved information, an example of which is shown in Fig. 1. Two cases are plotted, one assuming oxygen as the impurity and the other assuming iron as the contaminant. Despite differences having to do with the nature of the impurity, it can be seen that there is no strong central accumulation, but rather a general increase of Z_{eff} with time throughout the plasma. Data taken over a wide range of plasma currents indicate, by

comparison with resistivity measurements mentioned below, that the principal impurities present at low currents are light impurities (or a mixture of light and heavy impurities), while heavy impurities dominate at high currents.

A third common method of measuring Z_{eff} is to measure the plasma resistance and to relate this directly to Z_{eff} by the Spitzer formula [9], assuming T_e and n_e are known and including both neoclassical terms to account for trapped particles not carrying current and the bootstrap current. These corrections decrease Z_{eff} by 20 to 30% below the uncorrected Z_{eff}^{Sp}. While this procedure sounds straightforward, there are a number of complications. First of all, only the overall plasma resistance is measured; but the resistivity is a function of radius

$$R_p(r) = \frac{V_p}{2\pi R\, J(r)} ,$$

where $R_p(r)$ is the plasma resistivity, V_p is the plasma voltage drop induced by the transformer, R is the major radius, and J(r) is the current density in the plasma. Upon locating the mode-rational surfaces [10] (q = 1, 2) by means of spatially resolved x-ray fluctuation measurements, it is possible to infer the current density profile of the plasma. However, the Z_{eff} obtained depends sensitively upon the exact radial location of the q=2 surface, as shown in Fig. 2. The Z_{eff} one gets also depends somewhat on the impurity model, i.e. the impurity species and the ionization states as a function of radius. Another uncertainty inherent in this measurement arises from assuming that all resistance comes from collisions. Plasma turbulence also causes resistance which cannot be separated from the measurements, and so an overestimate of Z_{eff} results.

A fourth method used to determine Z_{eff} is to measure the charge-exchange energy spectrum of injected ions as they slow down in the plasma. Upon slowing down, their pitch angle with respect to the magnetic field changes due to scattering by impurity ions (as well as by H^+ ions). By the time these ions have been scattered by 90° from their injected direction, their energy distribution is a function of Z_{eff}, which can be calculated by means of the Fokker-Planck equation. The result can be compared with experiment, as shown in Fig. 3 for scattering from the center of the plasma. Recently, nonlocal calculations have been made which take into account scattering all along the chord viewed by the charge-exchange analyzer, and which assume a radial dependence for Z_{eff}.

Fig. 3

This scattering technique seems to be straightforward, but there are difficulties both with the theory and the experimental measurements. The major theoretical unknown is that of trapped particle effects. The Fokker-Planck calculations do not, at present, take into account ion orbit trapping which leads to a radial variation in the ion scattering. This can be important, since ions scattered by $\sim 90°$ are trapped; and it is these ions which are energy analyzed to determine Z_{eff}. Experimentally, the number of injected particles and the background neutral density must both be known for accurate calibration. For this purpose it is necessary to measure the number of charge-exchanged beam ions as a function of energy, both parallel and perpendicular to magnetic field lines.

4. Oxygen Discharge Pre-cleaning

Encouraged by the results of laboratory tests [4] using glow discharges, we have tried discharge pre-cleaning in ORMAK. As with previous discharge pre-cleaning which used H_2 gas, this cleaning involves 120-Hz intermittent

cathode-less discharges run in the same manner as regular tokamak shots, but with much reduced fields, current, and duration.

The results of switching from H_2 to O_2 discharge pre-cleaning [6] are shown in Fig. 4 for shots of equal plasma current. Ion and electron temperatures increased, there was an increase in plasma density, and there was less H_β and C III refluxing light. The carbon concentration decreased with continued discharge pre-cleaning and was believed to be below 1%. A comparison between the lines observed with H_2 and O_2 pre-cleaning is shown in Fig. 5. Note that with O_2 pre-cleaning the carbon lines disappeared and many higher ionization states of oxygen were present, indicating higher electron temperatures.

It is not clear how oxygen pre-cleaning affected the amount of oxygen in the plasma. Figure 6 is a record of the oxygen lines O III - O VI as a function of time during the discharge. In each case oxygen lines were "burned" through faster and their peaks were lower with O_2 pre-cleaning as opposed to H_2 pre-cleaning.

Similar comparisons between H_2 and O_2 discharge pre-cleaning showed Au I, Fe II, Be II, and Si III impurity ionization states to be reduced throughout the discharge. Under the wall conditions tested, O_2 discharge cleaning was effective in removing several impurity species, higher electron and ion temperatures were obtained, plasma currents were increased, and the operating parameter window was enlarged.

5. Power to the Wall and Z_{eff} Scaling

The integrated flux of particles and photons to the wall was monitored by a pyroelectric detector [12]. The response time of this detector was about 100 μsec, so that power measurements as a function of time were

possible. Most of the power was emitted as line radiation, with a smaller but nonnegligible fraction as charge-exchanged neutrals. Power measurements as a function of time are shown in Fig. 7 for three different plasma currents. During the middle portion of the discharge, when power balances were in equilibrium, 60-75% of the power reached the walls, the remainder being deposited on the limiter. The top (I_p = 140 kA) curve in Fig. 7 shows an abrupt increase at ~ 50 msec due to an injection of silicon. This silicon was injected by a pulse of the Thomson scattering laser striking a glass dump; it caused a power burst as a result of increased line radiation.

A plot of $Z_{eff} \times \bar{n}_e$ vs the plasma current, where Z_{eff} is the central value, is shown in Fig. 8. The shaded area encloses values of Z_{eff}^{Sp} derived directly from measurements of the plasma resistance [13]. The bottom line represents data from x-ray measurements. Since $Z_{eff} \times \bar{n}_e$ scales linearly with I_p, $Z_{eff} \sim I_p/\bar{n}_e$, i.e. Z_{eff} increases with plasma current and decreases with plasma density, indicating a constant amount of impurities at a given power level.

6. Summary

Attempts have been made to correlate impurities on the surface of the ORMAK liner with plasma impurities. At present neither surface studies nor plasma impurity studies are capable of shot-to-shot measurements, so that results to date are necessarily qualitative. The clearest correlations are those between H_2 and O_2 discharge pre-cleaning, where both wall contaminants (as tested in the laboratory) and plasma contamination spectra were observed to change. If more detailed comparisons are to be made, much work must be done to develop both surface physics and plasma impurity diagnostics.

7. Acknowledgments

We would like to thank W. R. Wing, J. A. Rome, and R. C. Isler for valuable discussions; J. L. Dunlap for data on location of the mode-rational surfaces; and R. E. Clausing and L. C. Emerson for AES analysis of various materials removed from ORMAK. P. H. Edmonds and H. E. Ketterer were responsible for machine operation. We gratefully acknowledge the continuing support of L. A. Berry and J. F. Clarke in carrying out these experiments.

References

[1] J. E. Simpkins, Proc. 5th Symposium on Engineering Problems of Fusion Research, Princeton University (1973) p. 385.

[2] R. J. Colchin et al., J. Nucl. Mater. 53 (1974) 25.

[3] R. E. Clausing et al., paper in these proceedings.

[4] R. E. Clausing et al., J. Vac. Sci. Technol. 13, No. 1 (1976).

[5] L. A. Berry et al., Plasma Physics and Controlled Nuclear Fusion Research, Vol. I (IAEA, Vienna, 1975) p. 101.

[6] R. V. Neidigh and L. J. Nugent, Bull. Am. Phys. Soc. 20 (1975) 1300.

[7] T. F. Stratton in Plasma Diagnostic Techniques (Academic Press, Inc., New York, 1965) ed. by R. H. Huddleston and S. L. Leonard, p. 359.

[8] W. R. Wing, Bull. Am. Phys. Soc. 18 (1973) 1254.

[9] L. Spitzer, Jr., Physics of Fully Ionized Gases, 2nd ed., (John Wiley, N. Y., 1962).

[10] L. A. Artsimovich, Nucl. Fusion 12 (1972) 215.

[11] L. A. Berry et al., Plasma Physics and Controlled Nuclear Fusion Research, Vol. 1 (IAEA, Vienna, 1974) p. 113.

[12] C. E. Bush et al., Bull. Am. Phys. Soc. 20 (1975) 1299.

[13] M. Murakami et al., Bull. Am. Phys. Soc. 20 (1975) 1299.

Table I. ORMAK Impurities

Element	Origin	Element Abundance (% n_e)
He	diagnostics	trace
Be	x-ray window	< 1.0
C	pump oil	> 5.0 → < 1.0
N	air	trace
O	discharge cleaning	1-2
Na, Cl, Ca	perspiration	< 0.1
Si	quartz windows	< 1.0
S	abundant element	~ 0.1
Cr, Mn, Ni	304 SS	
Fe	304 SS	< 1.0
Cu	injectors	
Ag	injectors	
W	limiter	
Pt	liner plate	
Au	liner plate	
many unidentified spectral lines		

FIGURE CAPTIONS

Fig. 1. Time evolution of Z_{eff} profiles measured by a PIN diode array for I_p = 175 kA discharges. Oxygen was assumed to be the impurity in the left-hand plot and iron was assumed on the right. Upward-pointing arrows indicate maximum possible Z_{eff}.

Fig. 2. Values of Z_{eff} as a function of radius for four positions of the q = 2 mode-rational surface. Although Z_{eff} is sensitive to the position of the q = 2 surface, it is relatively insensitive to the q = 1 location.

Fig. 3. Parallel and perpendicular energy distributions of captured beam ions as they slow down in energy and scatter in pitch angle. The best data fit gives $Z_{eff} \simeq 4$.

Fig. 4. Comparison of oxygen and hydrogen discharge pre-cleaning on plasma characteristics. Plots on the left show increases in the plasma temperature and density after oxygen pre-cleaning, and plots on the right show decreases in H_β and C III light.

Fig. 5. Spectrum of strong lines in the ultraviolet (10-300 Å) after hydrogen and oxygen discharge pre-cleaning. Fe XV and Fe XXII lines appear only after O_2 discharge cleaning. The Fe XXII line appears as a faint smudge. Hundreds of weaker lines are not reproduced.

Fig. 6. Spectral intensity (normalized by the electron density) of several oxygen lines during the first 20 msec of hydrogen and oxygen pre-cleaned discharges.

Fig. 7. Power to the wall as a function of time for plasma currents of 140, 122, and 100 kA. The corresponding power inputs to the plasma were 411, 333, and 234 kW.

Figure Captions (cont.)

Fig. 8. $Z_{eff} \times \bar{n}_e$ as a function of the plasma current. The shaded area represents the range of Z_{eff}^{Sp} as derived from the Spitzer resistivity formula with no allowance for trapped particles or bootstrap currents. The dashed line is a fit to Z_{eff}^{x} determined from x-ray measurements. Open circles are for oxygen, solid circles are for iron, and triangular points indicate that an impurity saturated plasma is required for the assumed impurity species.

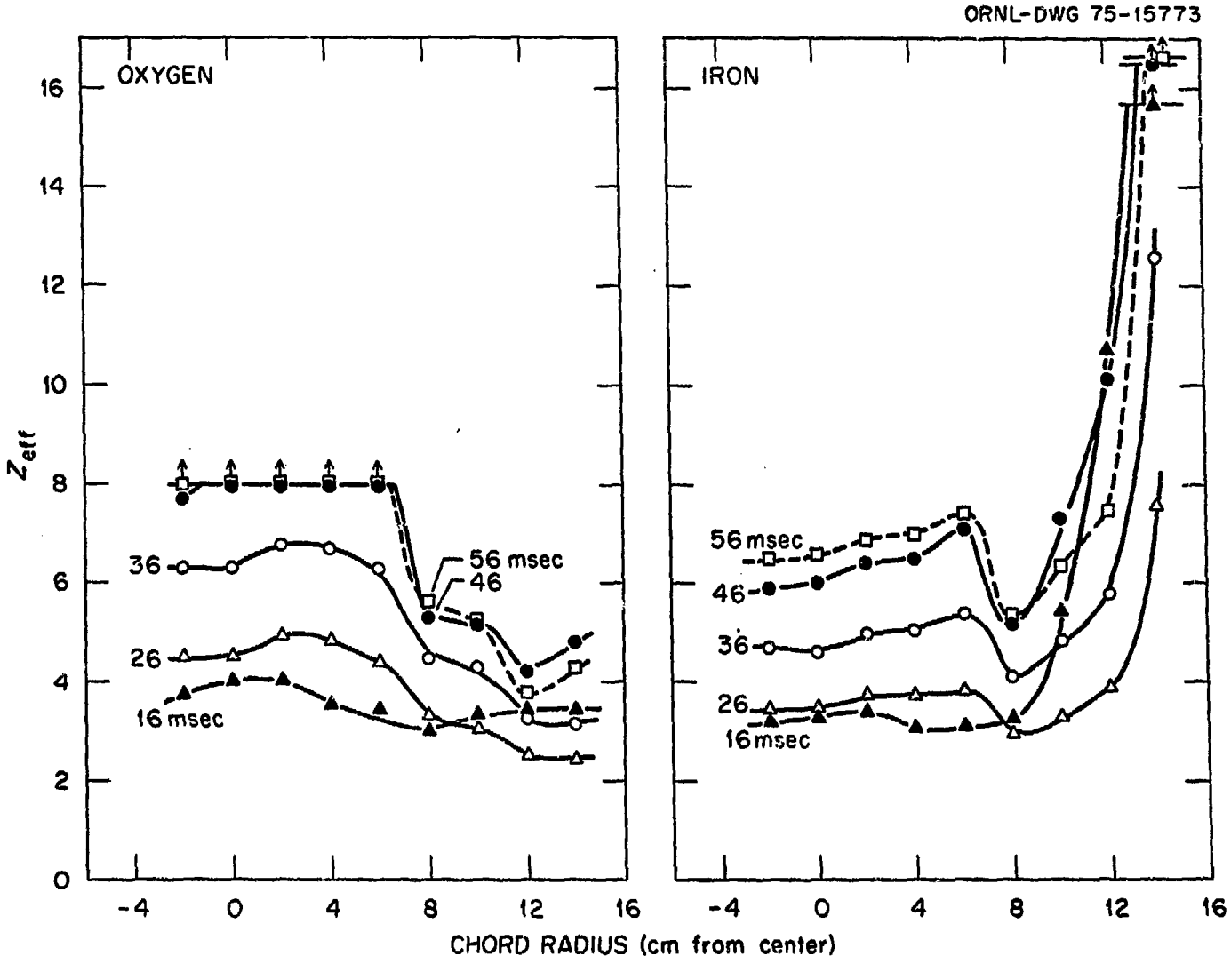
ORNL-DWG 75-15773
OXYGEN
IRON
Z_{eff}
56 msec
46
36
26
16 msec
CHORD RADIUS (cm from center)

ORNL-DWG 76-3107

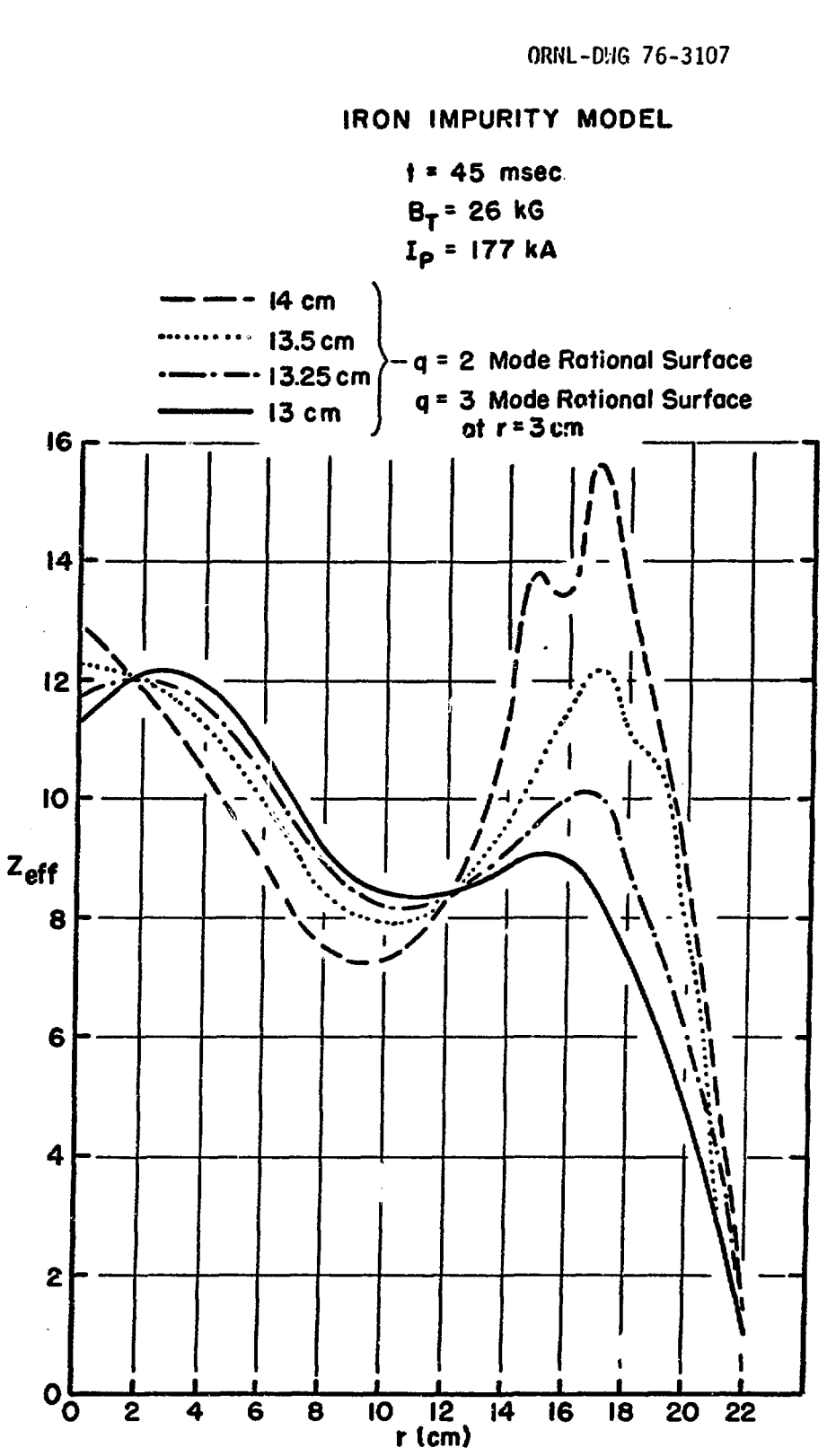

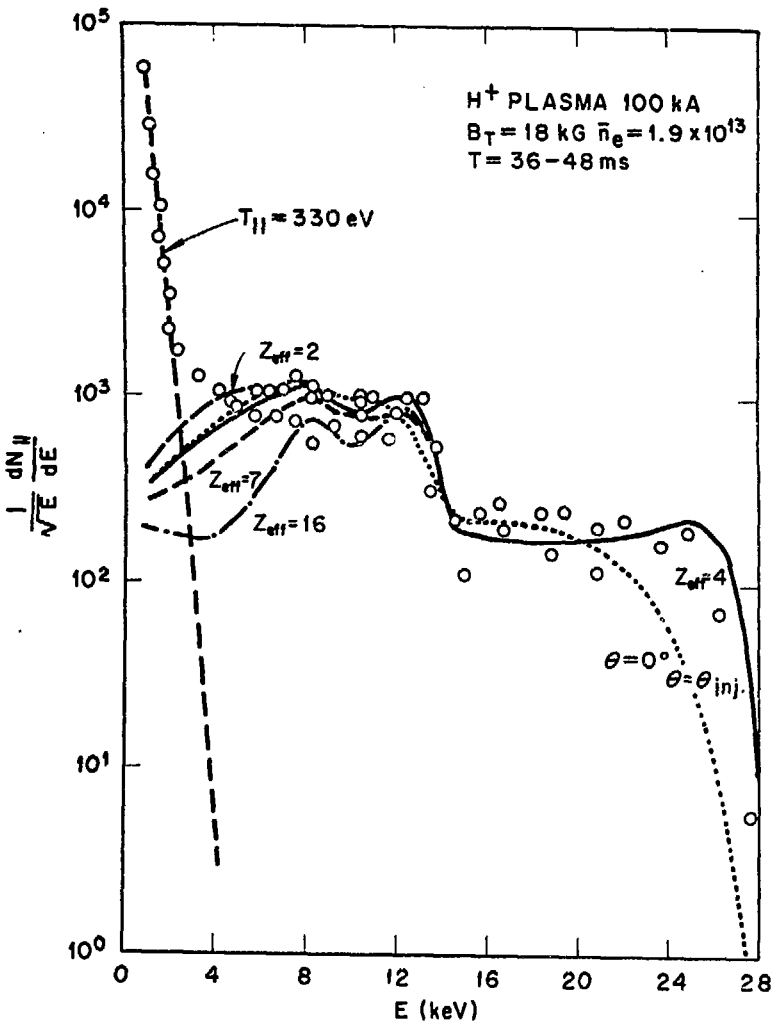
H+ PLASMA 100 kA
BT = 18 kG n̄e = 1.9 x 10^13
T = 36–48 ms
T|| = 330 eV
Zeff = 2
Zeff = 7
Zeff = 16
Zeff = 4
θ = 0°
θ = θinj.
1/√E dN||/dE
E (keV)

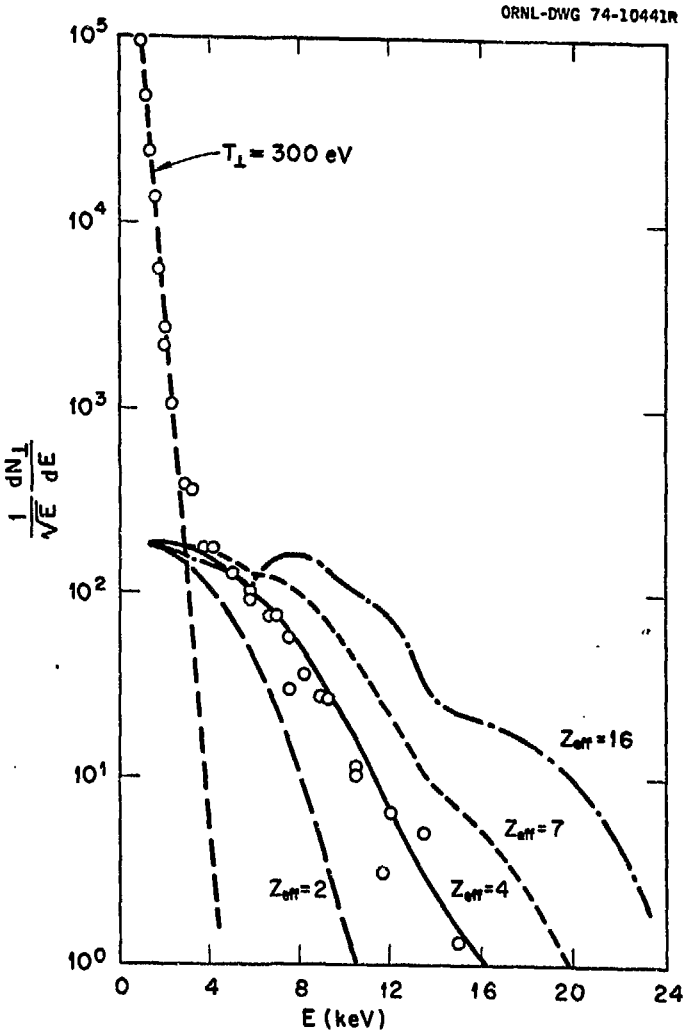
ORNL-DWG 74-10441R
T⊥ = 300 eV
Zeff = 16
Zeff = 7
Zeff = 2
Zeff = 4
1/√E dN⊥/dE
E (keV)

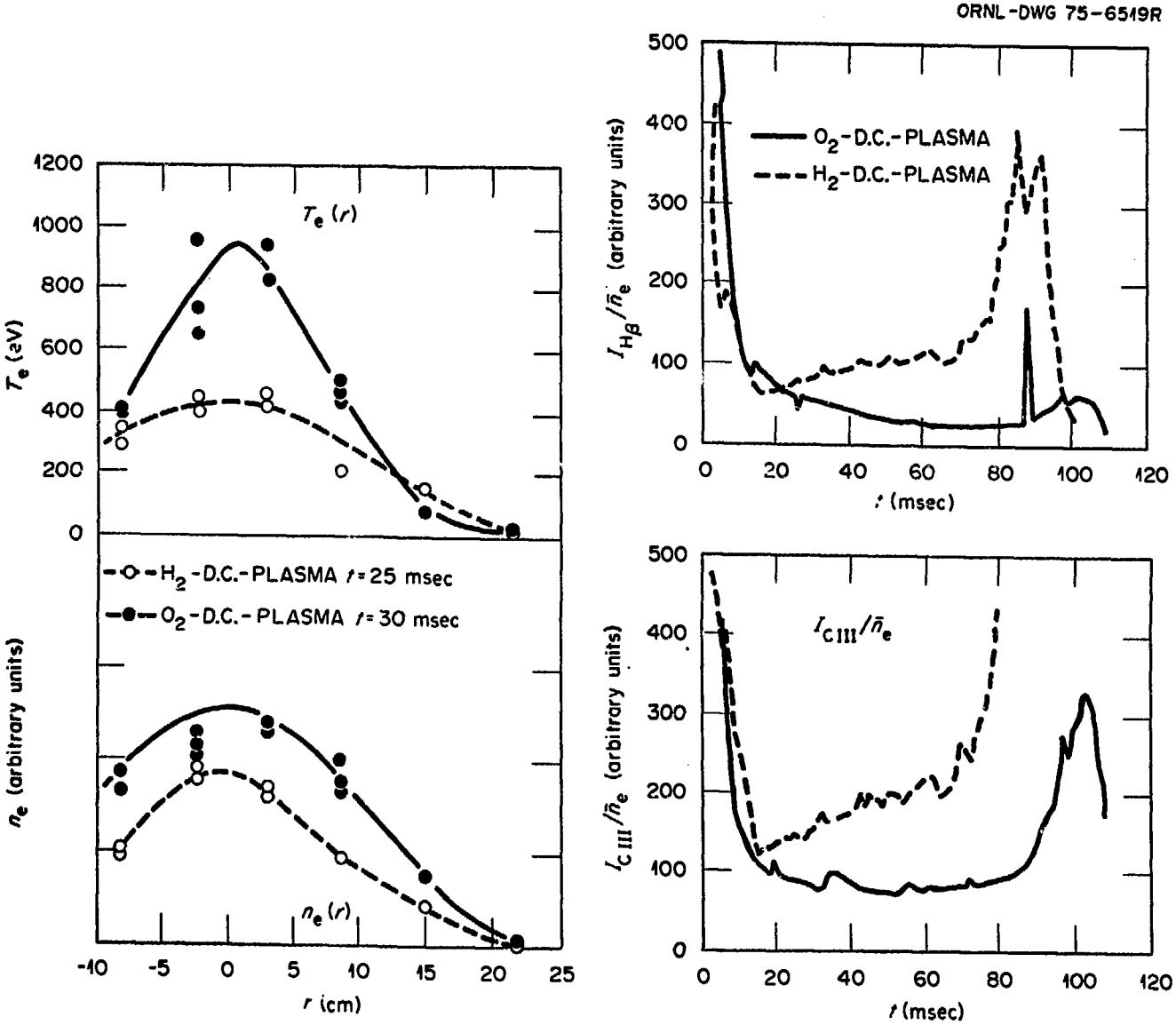
ORNL-DWG 75-6519R
T_e (eV)
$T_e(r)$
H_2-D.C.-PLASMA t=25 msec
O_2-D.C.-PLASMA t=30 msec
n_e (arbitrary units)
$n_e(r)$
r (cm)
$I_{H\beta}/\bar{n}_e$ (arbitrary units)
O_2-D.C.-PLASMA
H_2-D.C.-PLASMA
t (msec)
$I_{C\,III}/\bar{n}_e$
$I_{C\,III}/\bar{n}_e$ (arbitrary units)
t (msec)

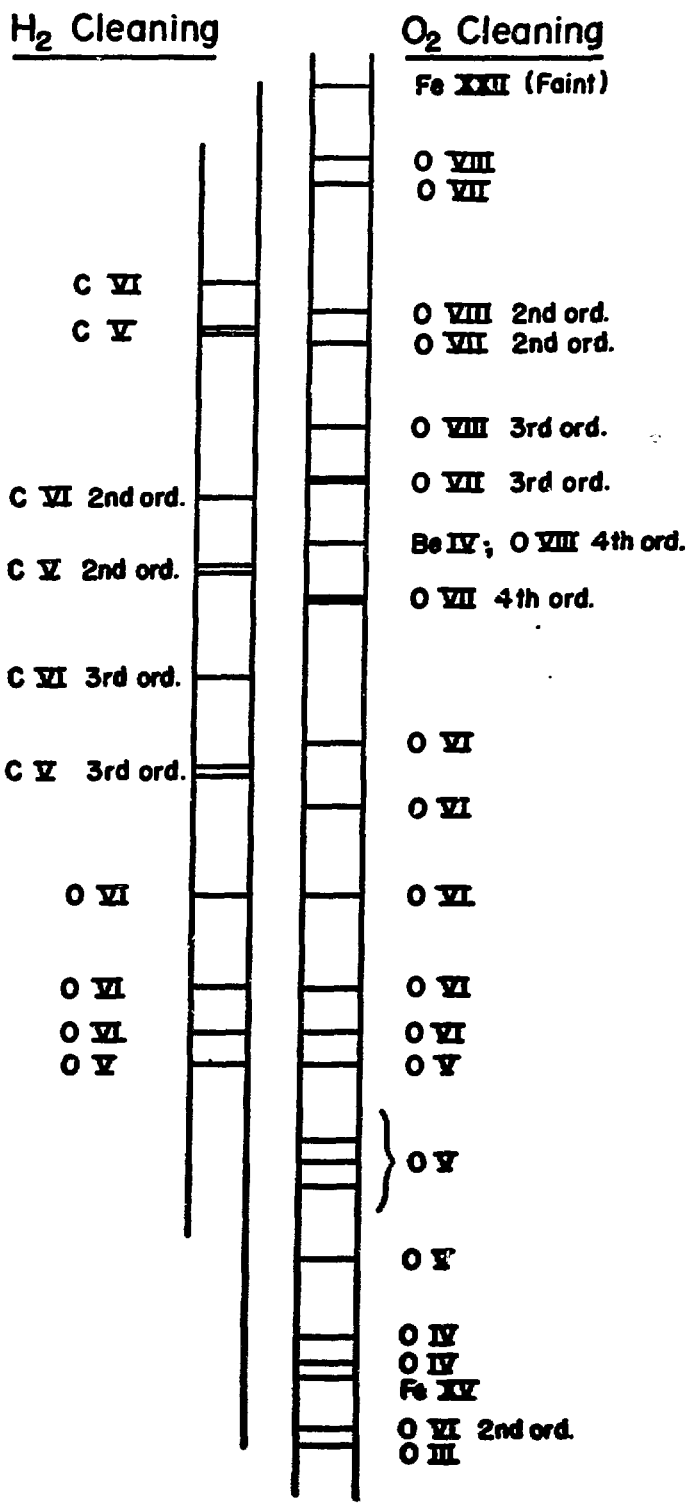
H2 Cleaning
O2 Cleaning
Fe XXII (Faint)
O VIII
O VII
C VI
C V
O VIII 2nd ord.
O VII 2nd ord.
O VIII 3rd ord.
C VI 2nd ord.
O VII 3rd ord.
Be IV; O VIII 4th ord.
C V 2nd ord.
O VII 4th ord.
C VI 3rd ord.
O VI
C V 3rd ord.
O VI
O VI
O VI
O VI
O VI
O VI
O V
O V
O V
O IV
O IV
Fe XV
O VI 2nd ord.
O III

ORNL-DWG 75-13176R

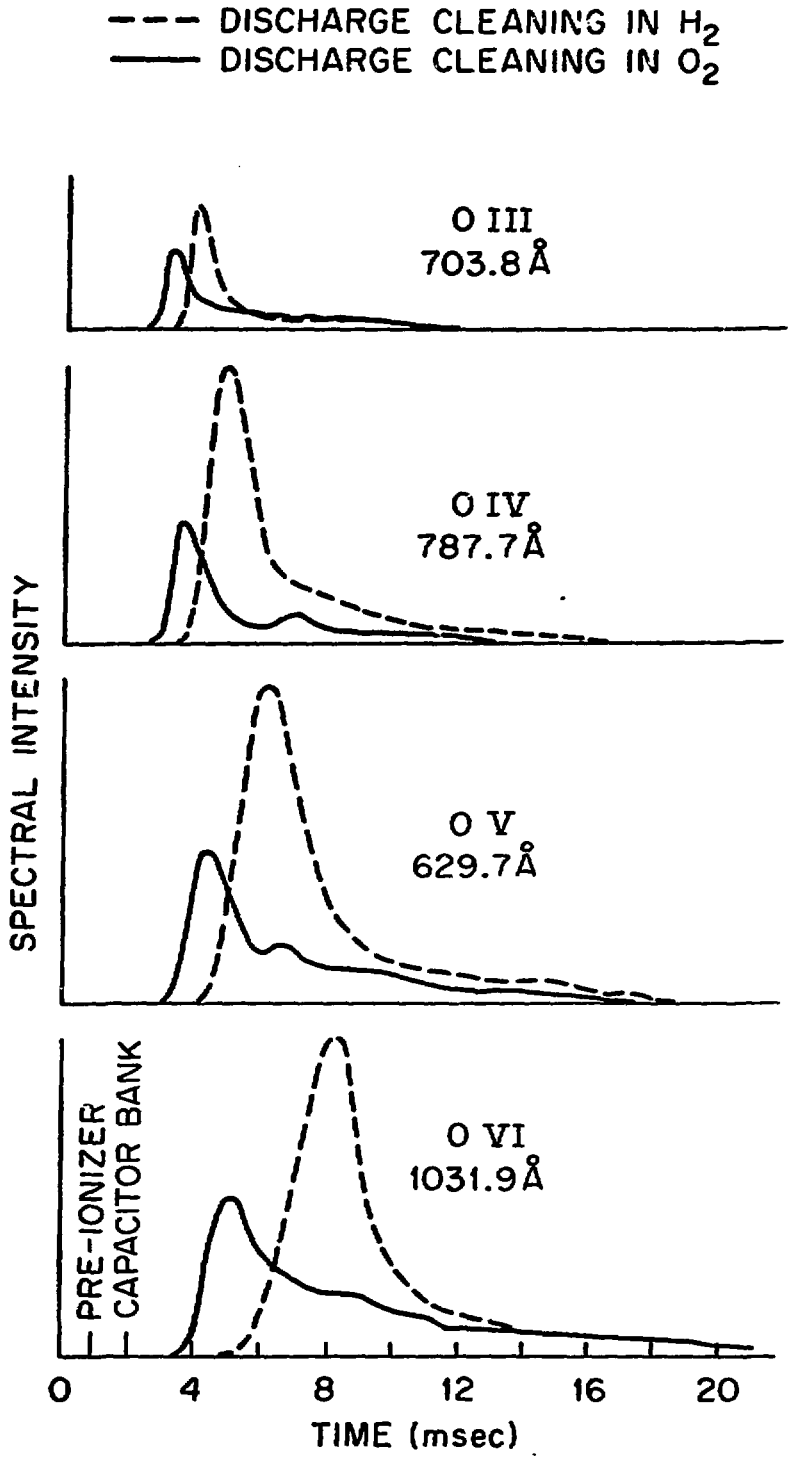

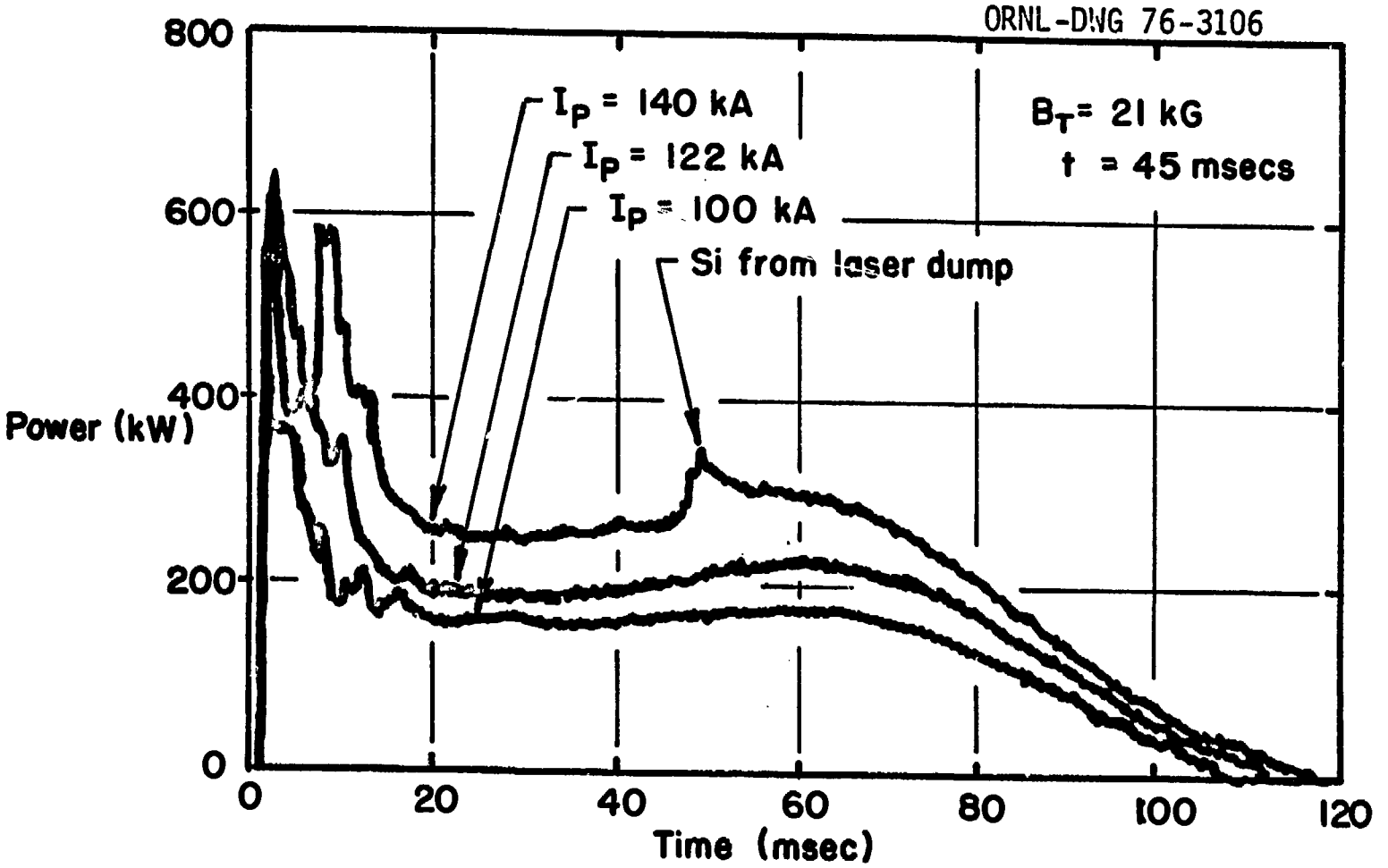
ORNL-DWG 76-3106
800
600
400
200
0
Power (kW)
I_P = 140 kA
I_P = 122 kA
I_P = 100 kA
Si from laser dump
B_T = 21 kG
t = 45 msecs
0
20
40
60
80
100
120
Time (msec)